IET Circuits, Devices & Systems

Research Article

IET Journals
The Institution of Engineering and Technology

Compact wide stopband microstrip diplexer with flat channels for WiMAX and wireless applications

ISSN 1751-858X
Received on 9th January 2020
Revised 7th March 2020
Accepted on 20th April 2020
E-First on 7th September 2020
doi: 10.1049/iet-cds.2020.0010
www.ietdl.org

Salah I. Yahya[1,2], Abbas Rezaei[3], Leila Nouri[4,5] ✉

[1]*Department of Software Engineering, Faculty of Engineering, Koya University, Koya KOY45, Kurdistan Region, Iraq*
[2]*Department of Communication and Computer Engineering, Cihan University-Erbil, Kurdistan Region, Iraq*
[3]*Department of Electrical Engineering, Kermanshah University of Technology, Kermanshah, Iran*
[4]*Institute of Research and Development, Duy Tan University, Da Nang 550000, Vietnam*
[5]*Faculty of Electrical– and Electronic Engineering, Duy Tan University, Da Nang 550000, Vietnam*
✉ *E-mail: leilanouri@duytan.edu.vn*

Abstract: This study presents a compact wide stopband microstrip diplexer which is designed based on a novel resonator structure. This novel resonator consists of a main hairpin cell loaded by a smaller hairpin and T-shaped cells. The presented diplexer operates at 3.46 and 4.75 GHz for IEEE 802.16 worldwide interoperability for microwave access (WiMAX) and IEEE802.11a Wireless LAN applications, respectively. The main advantages of the proposed diplexer are its flat channels, two wide bandwidths, attenuated harmonics, low insertion losses better than 0.18 dB, several transmission zeros and sharp frequency response. From first up to fifth harmonics of the proposed diplexer are well attenuated with the maximum harmonic level −20 dB. Meanwhile, the simulation results show that the presented design can suppress harmonics up to 44 GHz. In other words, the harmonics from the 1st up to 12th are suppressed. The group delay at both channels is lower than 1.1 ns, which is good for a microstrip diplexer. This good performance is obtained, while the overall area of the designed diplexer is only $0.037\lambda_g^2$. Based on the comparison results, the proposed diplexer has a compact size, the minimum group delay and a wide stopband rejection. The proposed diplexer is fabricated and measured. Both simulation and measurement results are in good agreement.

1 Introduction

Compact size and wide stopband play an important role in modern microstrip diplexer applications. Compact planar microstrip diplexers are important devices that are usually used to separate radio frequency signals in the modern communication systems. A high-performance diplexer is very attractive for wireless applications. Accordingly, several microstrip bandpass–bandpass diplexers have been reported in [1–15]. On the other hand, using a new resonator in the diplexer design is a significant advantage. Coupled open loops in [1], stub-loaded coupled open loops in [2], interdigital cells in [3], and stub-loaded U-shaped cells in [4, 5] have been used. The proposed diplexer in [6] has a novel structure consisting of step impedance cells, loops, coupled lines and low impedance sections. In [7], a microstrip diplexer has been achieved using three simple U-shape resonators integrated by coupled lines. Coupled step impedance cells [8], meandrous closed loops connected to interdigital structures [9], coupled spiral cells [10], meandrous line and patch cells [11] and engraved semi-patch cells [12] have been utilised to design the two-channel microstrip diplexers. The microstrip diplexer in [13] has been designed based on the slot line-loaded microstrip ring resonator. Similar to [1], the proposed diplexer in [14] has been designed using the coupled open loops. Finally, a three-coupled-line structure has been proposed to design a microstrip filter and a microstrip diplexer in [15]. However, this diplexer occupies a large area. The frequency response of a high-performance diplexer should be sharp with suppressed harmonics, flat passbands and low losses. However, the proposed diplexers in [1–15] have disadvantages in terms of group delay, size and losses. With the development of technology, the trend towards having a small size of electronic devices has been increased. The microstrip diplexers presented in [1–11] occupy large implementation areas. Another disadvantage of the reported diplexers in [1–11] is their large insertion losses. Having a stopband with attenuated harmonics is one of the most important factors of the filter and diplexer designs. However, the previous designs in [1–15] could not suppress the harmonics significantly. The best harmonic attenuation has been achieved in [12], which could only attenuate the first, second, and third harmonics. A microstrip device with non-flat group delay has the problem of pulse distortion [6]. Even though the group delay has a significant impact on the performance, the majority of the previous diplexers did not address this issue. The group delays are mentioned only in [6, 12, 15], which have high values. A dual closed-loop stepped impedance resonator has been used to design a microstrip diplexer in [16]. In [17], a compact microstrip diplexer including two bandpass filters (BPFs) with sharp passband has been fabricated. In [18], the stepped-impedance resonator has been used to design a microstrip diplexer. In [19], a microstrip diplexer with high isolation has been proposed based on a dual-mode substrate integrated waveguide resonator. However, it has a large size and losses. In [20], stub-loaded coupled lines have been used to design a miniaturised microstrip diplexer with relatively large group delay. The proposed diplexers in [16, 18] have large insertion losses. In [21], a compact microstrip diplexer with high isolation has been proposed for global system for mobile communications (GSM) applications. In [22], a wideband microstrip diplexer has been presented using an artificial neural network method.

This work presents a new microstrip diplexer, which can solve the problems of the previous diplexers. Our proposed diplexer has a small size, wide fractional bandwidths (FBWs), low insertion losses and high-frequency selectivity. Moreover, it has a very wide stopband rejection with several transmission zeros (TZs). The proposed resonator consists of a hairpin cell loaded by a smaller hairpin and a T-shaped cell coupled to spiral cells, which is presented for the first time in this work. It operates at 3.46 and 4.75 GHz for worldwide interoperability for microwave access (WiMAX) and wireless communication systems.

The design method is based on a mathematical analysis of the proposed resonator. Then, the most effective parameters in determining the resonator behaviour are found. An optimisation method is used to find the dimensions of the microstrip sections

based on the resonator behaviour extracted from the mathematical equations.

2 Design of the proposed diplexer

The hairpin cell is an appropriate choice to create a microstrip resonator. The narrow and wide parts of hairpin cells have inductance and capacitance features, respectively. To have more control over the frequency response and miniaturisation, it is possible to load several stubs inside the hairpin cell. Hence, a novel resonator with a compact size and a high degree of freedom to adjust the dimensions can be presented. Based on the above explanation, a novel stub-loaded resonator is proposed as shown in Fig. 1*a*. It includes a hairpin loaded by a T-shaped and a smaller hairpin cell. An approximated equivalent *LC* model of the proposed resonator is depicted in Fig. 1*b*. The narrow stubs l_1, l_2, l_3, l_4 are replaced by the inductances L_1, L_2, L_3, L_4, respectively. The patch cells C_1 and C_2 have capacitance features that are presented by two capacitors C_1 and C_2, respectively. The bents and steps are considered only at the frequencies >10 GHz [14]. Thus, their effects in the proposed model are ignored. The T-shaped stub is replaced by the inductor L_3 and the capacitor C_3 so that the wide stub with the width w has capacitance properties.

To show the impedance matching, we can calculate the *ABCD* matrix. The *ABCD* matrix of the proposed *LC* circuit can be calculated as follows:

$$\begin{aligned}
T &= \begin{bmatrix} A & B \\ C & D \end{bmatrix} \\
&= \begin{bmatrix} 1 & 0 \\ \mathrm{j}\omega C_1 & 1 \end{bmatrix} \times \begin{bmatrix} 1 & \mathrm{j}\omega L_1 \\ 0 & 1 \end{bmatrix} \times \begin{bmatrix} 1 & 0 \\ Y_2 & 1 \end{bmatrix} \times \begin{bmatrix} 1 & \mathrm{j}\omega L_4 \\ 0 & 1 \end{bmatrix} \times \begin{bmatrix} 1 & 0 \\ Y_3 & 1 \end{bmatrix} \\
&\quad \times \begin{bmatrix} 1 & \mathrm{j}\omega L_4 \\ 0 & 1 \end{bmatrix} \times \begin{bmatrix} 1 & 0 \\ Y_2 & 1 \end{bmatrix} \times \begin{bmatrix} 1 & \mathrm{j}\omega L_1 \\ 0 & 1 \end{bmatrix} \times \begin{bmatrix} 1 & 0 \\ \mathrm{j}\omega C_1 & 1 \end{bmatrix} \Rightarrow \\
T &= \begin{bmatrix} 1 & \mathrm{j}\omega L_1 \\ \mathrm{j}\omega C_1 & 1 - \omega^2 L_1 C_1 \end{bmatrix} \times \begin{bmatrix} 1 & \mathrm{j}\omega L_4 \\ Y_2 & 1 + \mathrm{j}\omega L_4 Y_2 \end{bmatrix} \\
&\quad \times \begin{bmatrix} 1 & \mathrm{j}\omega L_4 \\ Y_3 & 1 + \mathrm{j}\omega L_4 Y_3 \end{bmatrix} \times \begin{bmatrix} 1 & \mathrm{j}\omega L_1 \\ Y_2 & 1 + \mathrm{j}\omega L_1 Y_2 \end{bmatrix} \times \begin{bmatrix} 1 & 0 \\ \mathrm{j}\omega C_1 & 1 \end{bmatrix} \Rightarrow \\
T &= \begin{bmatrix} Z_D & \mathrm{j}\omega (L_4 + L_1 Z_A) \\ \mathrm{j}\omega C_1 + Y_2 Z_B & Z_A Z_B - \omega^2 C_1 L_4 \end{bmatrix} \\
&\quad \times \begin{bmatrix} Z_A & \mathrm{j}\omega (L_1 + L_4 Z_D) \\ (Y_3 + Y_2 Z_C) & \mathrm{j}\omega L_1 Y_3 + Z_D Z_C \end{bmatrix} \times \begin{bmatrix} 1 & 0 \\ \mathrm{j}\omega C_1 & 1 \end{bmatrix} \Rightarrow \\
T &= \begin{bmatrix} A_A & B_A \\ C_A & D_A \end{bmatrix} \times \begin{bmatrix} 1 & 0 \\ \mathrm{j}\omega C_1 & 1 \end{bmatrix} = \begin{bmatrix} A_A + \mathrm{j}\omega C_1 B_A & B_A \\ C_A + \mathrm{j}\omega C_1 D_A & D_A \end{bmatrix}
\end{aligned} \tag{1}$$

$$\begin{aligned}
Y_2 &= \mathrm{j}\omega C_2/(1 - \omega^2 L_2 C_2) \\
Y_3 &= \mathrm{j}\omega C_3/(1 - \omega^2 L_3 C_3) \\
Z_A &= 1 + \mathrm{j}\omega L_4 Y_2 \\
Z_B &= 1 - \omega^2 L_1 C_1 \\
Z_C &= 1 + \mathrm{j}\omega L_4 Y_3 \\
\text{where } Z_D &= 1 + \mathrm{j}\omega L_1 Y_2 \\
A_A &= Z_D Z_A + \mathrm{j}\omega (L_4 + L_1 Z_A)(Y_3 + Y_2 Z_C) \\
B_A &= \mathrm{j}\omega (L_1 + L_4 Z_D) Z_D + \mathrm{j}\omega (L_4 + L_1 Z_A)[\mathrm{j}\omega L_1 Y_3 + Z_D Z_C] \\
C_A &= [\mathrm{j}\omega C_1 + Y_2 Z_B] Z_A + (Y_3 + Y_2 Z_C)[Z_A Z_B - \omega^2 C_1 L_4] \\
D_A &= [\mathrm{j}\omega C_1 + Y_2 Z_B][\mathrm{j}\omega (L_1 + L_4 Z_D] \\
&\quad + [Z_A Z_B - \omega^2 C_1 L_4][\mathrm{j}\omega L_1 Y_3 + Z_D Z_C
\end{aligned}$$

In (1), ω is the angular frequency and Y_2 is an equivalent admittance of the patch cell C_2 with the stub with the physical length l_2. Similarly, Y_3 is the equivalent admittance of the T-shaped stub. Based on (1), the reflection coefficient of the introduced resonator is calculated as follows:

$$\begin{aligned}
\Gamma &= \frac{A + B - C - D}{A + B + C + D} \\
&= \frac{A_A + \mathrm{j}\omega C_1 B_A + B_A - C_A - \mathrm{j}\omega C_1 D_A - D_A}{A_A + \mathrm{j}\omega C_1 B_A + B_A + C_A + \mathrm{j}\omega C_1 D_A + D_A}
\end{aligned} \tag{2}$$

To have a perfect matching, the reflection coefficient should be zero. Accordingly, the condition of good impedance matching can be written as

$$\Gamma = 0 \Rightarrow A_A + \mathrm{j}\omega C_1 B_A + B_A - C_A - \mathrm{j}\omega C_1 D_A - D_A = 0 \tag{3}$$

If we can set the parameters so that they satisfy (3), then the perfect impedance matching will be achieved. Having the perfect impedance matching leads to a decrease in insertion losses. As presented in the recent equation, there is a high degree of freedom to have a good impedance matching. We can set the larger sections, e.g. main hairpin cell, as the desired and then tune the other internal stubs. By using this method, reducing the overall dimensions should be considered. Accordingly, the larger external hairpin cell should be small and the other dimensions must be tuned in accordance with it.

From the equivalent circuit of the proposed resonator, the input impedance (Z_{in}) can be calculated as follows:

$$Z_{\mathrm{in}} = \frac{\left(\frac{[\frac{(Z_1 Z_2/(Z_1 + Z_2) + Z_4) Z_3}{Z_1 Z_2/(Z_1 + Z_2) + Z_4 + Z_3} + Z_4] Z_2}{\frac{(Z_1 Z_2/(Z_1 + Z_2) + Z_4) Z_3}{Z_1 Z_2/(Z_1 + Z_2) + Z_4 + Z_3} + Z_4 + Z_2} + \mathrm{j}\omega L_1\right) \times \frac{1}{\mathrm{j}\omega C_1}}{\frac{[\frac{(Z_1 Z_2/(Z_1 + Z_2) + Z_4) Z_3}{Z_1 Z_2/(Z_1 + Z_2) + Z_4 + Z_3} + Z_4] Z_2}{\frac{(Z_1 Z_2/(Z_1 + Z_2) + Z_4) Z_3}{Z_1 Z_2/(Z_1 + Z_2) + Z_4 + Z_3} + Z_4 + Z_2} + Z_1} \tag{4}$$

where

$$\begin{aligned}
Z_1 &= \mathrm{j}\omega L_1 + \frac{1}{\mathrm{j}\omega C_1}; \quad Z_2 = \mathrm{j}\omega L_2 \\
&+ \frac{1}{\mathrm{j}\omega C_2}; \quad Z_3 = \mathrm{j}\omega L_3 + \frac{1}{\mathrm{j}\omega C_3}; \quad Z_4 = \mathrm{j}\omega L_4
\end{aligned}$$

In the above equation, ω is an angular resonance frequency. To have simpler calculations, we can rewrite (4) as follows:

$$Z_{\mathrm{in}} = \frac{(Z_a + \mathrm{j}\omega L_1) \times \frac{1}{\mathrm{j}\omega C_1}}{Z_a + Z_1} \Rightarrow Z_{\mathrm{in}} = \frac{Z_a + \mathrm{j}\omega L_1}{\mathrm{j}\omega C_1 (Z_a + Z_1)} \tag{5}$$

where

$$Z_a = \frac{[Z_b + Z_4] Z_2}{Z_b + Z_4 + Z_2}; \quad Z_b = \frac{(Z_1 Z_2/(Z_1 + Z_2) + Z_4) Z_3}{Z_1 Z_2/(Z_1 + Z_2) + Z_4 + Z_3}$$

The odd mode resonance frequency can be obtained by $Z_{\mathrm{in}} = 0$, while the even mode resonance frequency can be calculated by $(1/Z_{\mathrm{in}}) = 0$. Accordingly, for the even mode $\mathrm{j}\omega C_1 (Z_{\mathrm{b}} + Z_1) = 0$, therefore

$$\begin{aligned}
Z_b = -Z_1 \Rightarrow \frac{(Z_a + \mathrm{j}\omega_{\mathrm{e}} L_4) \times (\mathrm{j}\omega_{\mathrm{e}} L_2 + \frac{1}{\mathrm{j}\omega_{\mathrm{e}} C_2})}{Z_a + \mathrm{j}\omega_{\mathrm{e}} L_4 + \mathrm{j}\omega_{\mathrm{e}} L_2 + \frac{1}{\mathrm{j}\omega_{\mathrm{e}} C_2}} = -\mathrm{j}\omega_{\mathrm{e}} L_1 - \frac{1}{\mathrm{j}\omega_{\mathrm{e}} C_1} \\
\Rightarrow \frac{-\omega_{\mathrm{e}}^2 L_2 Z_a C_2 - \mathrm{j}\omega_{\mathrm{e}}^3 L_2 L_4 C_2 + Z_a + \mathrm{j}\omega_{\mathrm{e}} L_4}{\mathrm{j}\omega_{\mathrm{e}} C_2 Z_a - \omega_{\mathrm{e}}^2 C_2 L_4 - \omega_{\mathrm{e}}^2 C_2 L_2 + 1} = \frac{\omega_{\mathrm{e}}^2 L_1 C_1 - 1}{\mathrm{j}\omega_{\mathrm{e}} C_1}
\end{aligned} \tag{6}$$

In (6), ω_{e} is the even mode angular resonance frequency. Similarly, the odd mode resonance frequency can be calculated as follows:

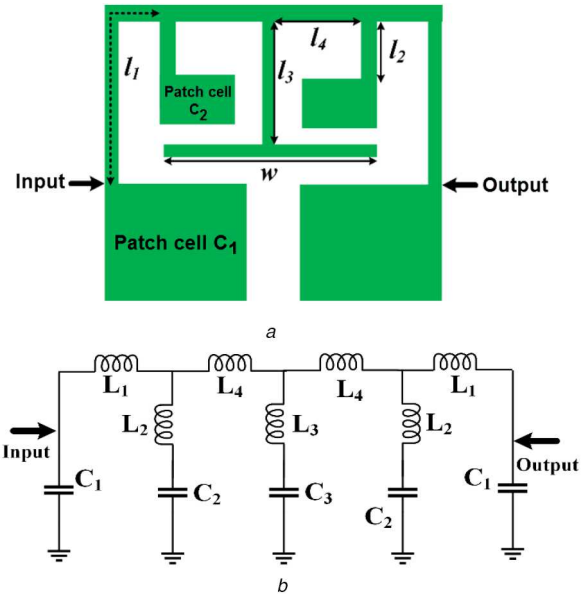

Fig. 1 *Proposed resonator*
(a) Physical structure, ***(b)*** Equivalent LC circuit

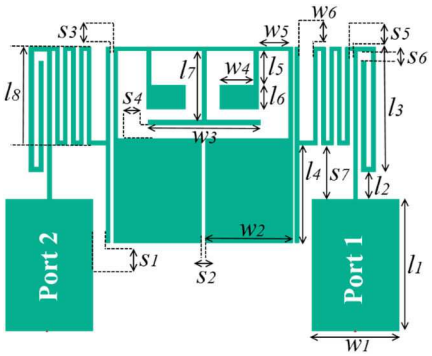

Fig. 2 *Layout of the presented BPF* ($s_1 = 0.26$ *mm*, $s_2 = 0.08$ *mm*, $s_3 = 0.08$ *mm*, $s_4 = 0.28$ *mm*, $s_5 = 0.07$ *mm*, $s_6 = 0.2$ *mm*, $s_7 = 1.13$ *mm*, $w_1 = 1.78$ *mm*, $w_2 = 1.78$ *mm*, $w_3 = 2.28$ *mm*, $w_4 = 0.7$ *mm*, $w_5 = 0.6$ *mm*, $w_6 = 0.3$ *mm*, $l_1 = 2.73$ *mm*, $l_2 = 0.56$ *mm*, $l_3 = 2.6$ *mm*, $l_4 = 2$ *mm*, $l_5 = 0.7$ *mm*, $l_6 = 0.5$ *mm*, $l_7 = 1.43$ *mm and* $l_8 = 2$ *mm*)

$$Z_b = -\mathrm{j}\omega_o L_1 \Rightarrow \frac{(Z_a + \mathrm{j}\omega_o L_4) \times (\mathrm{j}\omega_o L_2 + \frac{1}{\mathrm{j}\omega_o C_2})}{Z_a + \mathrm{j}\omega_o L_4 + \mathrm{j}\omega_o L_2 + \frac{1}{\mathrm{j}\omega_o C_2}} = -\mathrm{j}\omega_o L_1 \tag{7}$$

In (7), ω_o is the odd mode angular resonance frequency. The even and odd modes of angular resonance frequencies can be located at the desired points by adjusting the values of inductors and capacitors in accordance with (6) and (7), respectively.

The proposed resonator is developed to achieve a BPF as shown in Fig. 2.

The BPF consists of the proposed resonator and spiral cells, which has an area of 8 mm × 5.95 mm. The spiral cells have inductance features while they occupy a small area. The frequency response of this filter and its group delay are presented in Figs. 3*a* and *b*, respectively. The proposed filter has high selectivity with a good stopband rejection. It works at 5 GHz, where −3 dB cut-off frequencies are located at 4.4 and 5.6 GHz. The proposed BPF has several TZs, which improved its stopband properties. The TZs are: (7.25 GHz, −51 dB), (10.3 GHz, −38.7 dB), (12.3 GHz, −40 dB), (17.35 GHz, −30 dB), (18.55 GHz, −29.3 dB), (19.35 GHz, −31.5 dB), (22.2 GHz, −43 dB), and (26.9 GHz, −24.1 dB). It has 0.18

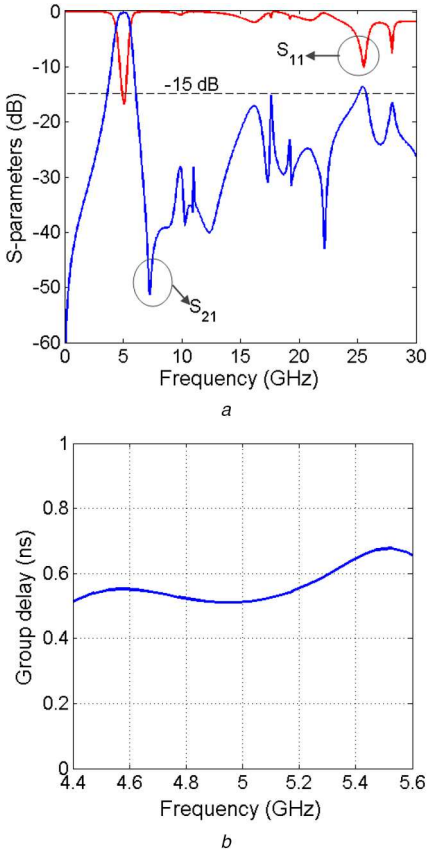

Fig. 3 *Proposed BPF*
(a) Frequency response, ***(b)*** Group delay

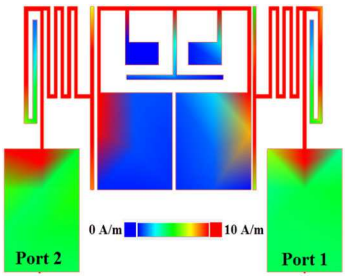

Fig. 4 *Current density distribution of the proposed BPF at 5 GHz*

dB insertion loss and 16.5 dB return loss. As depicted in Fig. 3*a*, the harmonics of the proposed filter are attenuated up to 25 GHz with the maximum harmonic level −15 dB. Therefore, it can attenuate from the first harmonic up to the fifth harmonic. Another advantage of this BPF is the wide FBW 24%.

To find the most important section of the BPF affecting the frequency response, we can use the current density distribution. Fig. 4 depicts the current density distribution at the surface of the proposed BPF at 5 GHz.

As presented in Fig. 4, the internal stubs are less significant than the spiral and main hairpin cells. These patch sections are used to miniaturise the overall area in λ_g^2. If we reduce the patch area, the resonance frequency will be increased. We changed the overall dimensions of the BPF shown in Fig. 2 with the scales of 90% (scale 0.9:1), 110% (scale 1.1:1), 150% (scale 1.5:1) and 200% (scale 2:1). The transmission parameter (S_{21}) and return loss (S_{11}) as functions of the BPF scales are presented in Figs. 5*a* and *b*, respectively. As presented in Fig. 5*a*, by decreasing the overall dimensions the frequency response is shifted to the right but the FBW is wider for a smaller device. By knowing the behaviour of the proposed resonator and BPF, a diplexer is designed by integrating two BPFs, as presented in Fig. 6. All dimensions of the presented diplexer are in mm. Also, the larger BPF (BPF2) is 1.3 times bigger than the smaller BPF (BPF1 shown in Fig. 6).

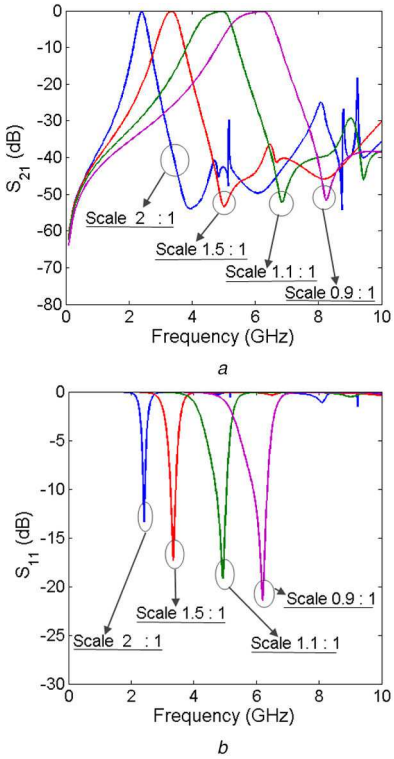

Fig. 5 *S-parameters of the proposed BPF as functions of overall dimensions*
(a) S_{21}, ***(b)*** S_{11}

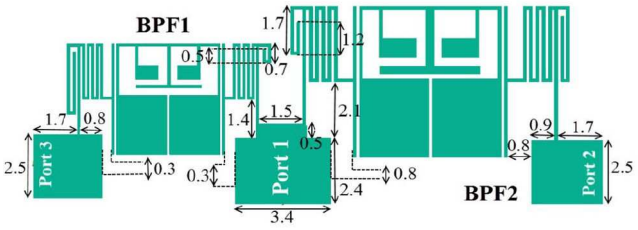

Fig. 6 *Proposed diplexer layout, scale (BPF2: BPF1) = (1.3:1)*

The current density distributions at the surface of the proposed diplexer are shown in Fig. 7*a* (for 3.46 GHz) and Fig. 7*b* (for 4.75 GHz). It is obvious from Fig. 7 that our proposed diplexer is affected by the larger hairpin and spiral dimensions.

3 Measurement results and comparison

EM simulator of ADS software and N5230A network analyser are used to simulate the presented diplexer and measure the fabricated structure, respectively. To fabricate the proposed design, we used a substrate with the following characteristics:

- Type: RT/Duroid 5880
- Loss tangent $\tan(\delta) = 0.0009$
- $\varepsilon_r' = 2.2$
- Thickness $h = 0.031''$ (0.787 mm)

The measured and simulated transmission parameters are presented in Fig. 8*a*. As shown in this figure, the frequency response is sharp with the attenuated harmonics and several TZs. Fig. 8*b* depicts the measured (from DC up to 20 GHz) and simulated (from DC up to 45 GHz) common port return loss (S_{11}) and isolation (S_{23}). The measured and simulated return losses from each port (S_{33} and S_{22}) are shown in Fig. 8*c*.

The simulation and measurement results are in good agreement. However, due to copper loss and junction loss, the measured losses are a little more than the simulated losses. The first passband is from 3.27 up to 3.84 GHz with the resonance frequency 3.46 GHz. The second passband is from 4.28 up to 5.56 GHz with the

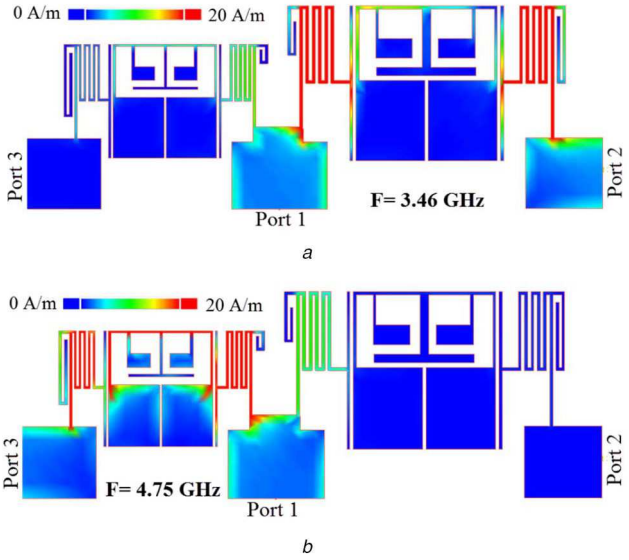

Fig. 7 *Current density distribution at the surface of the proposed diplexer at*
(a) 3.46 GHz, ***(b)*** 4.75 GHz

resonance frequency 4.75 GHz. The area of the proposed diplexer is $20.3\,\text{mm} \times 7.28\,\text{mm} = 0.037\,\lambda_g^2$, where λ_g is the calculated guided wavelength at 3.46 GHz. The isolation of the introduced diplexer is >20 dB up to 25 GHz. The simulated insertion loss at the first channel is <0.12 dB and the second channel is <0.18 dB. The return losses are 21 dB (at the lower channel) and 17 dB (at the upper channel). The proposed diplexer has the wide FBWs at both channels so that they are 16.4% (for the first channel) and 26% (for the second channel). Fig. 9 shows the fabricated diplexer. A comparison between this work and the previous diplexers is presented in Table 1. As shown in Table 1, the proposed diplexer has a compact electrical size with wide channels and low insertion losses.

In Table 1, indexes 1 and 2 are related to the lower and upper channels, respectively. The presented diplexers in [12–14, 17, 18,

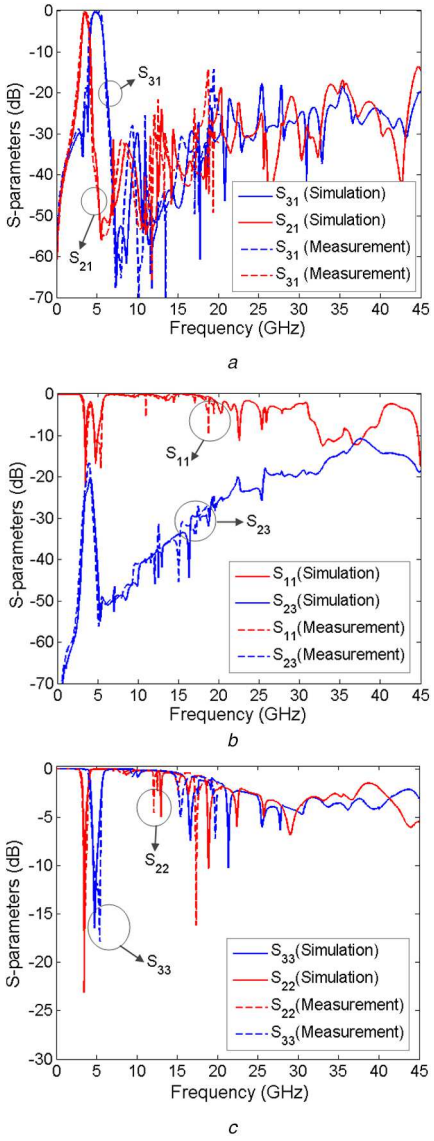

Fig. 8 *Measured and simulated frequency responses*
(a) S_{21} and S_{31}, ***(b)*** Common port return loss and isolation, ***(c)*** S_{22} and S_{33}

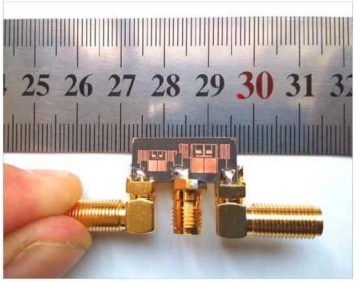

Fig. 9 *Fabricated diplexer*

21] are smaller than this work. However, they could not attenuate the harmonics well while they have narrow channels with higher group delays. On the other hand, the best insertion losses at both channels are obtained in this work and [22]. The best return losses are obtained in [8, 22]. However, our diplexer has better group delay and harmonic attenuation. The simulation results show that the harmonics are well attenuated up to 44 GHz with the maximum harmonic level −17 dB. The simulated and measured harmonics are suppressed up to 20 GHz with the maximum harmonic level −20 dB. Therefore, first, second, third, fourth, and fifth harmonics are well suppressed. The stopband property of this work is compared with the previous diplexers in Table 2. As depicted in Table 2, we could obtain the best stopband in comparison with the previous works. The designed diplexer has several TZs, which improved the stopband properties so that there are 38 TZs at the stopband of the proposed diplexer.

A microstrip diplexer with a linear phase or constant group delay at desired frequencies does not distort the signal that propagates through it. Moreover, having low group delay means that the measured time required for a signal to propagate through the diplexer is low. Another advantage of our diplexer is its flat passbands with low group delay. The simulated and measured group delay curves for the first and second channels are depicted in Figs. 10*a* and *b*. The measured group delay is better than 1.12 ns (at the first channel) and 0.9 ns (at the second channel). The group delay of our diplexer is compared with the group delays of the previous diplexers and filters, as shown in Table 3. It is obvious that we could achieve the best group delay, even though obtaining

Table 1 Comparison between this work and previous diplexers in terms of the insertion losses (IL_1, IL_2), return losses (RL_1, RL_2), fractional bandwidths (FBW_1, FBW_2), resonance frequencies (f_1, f_2) and area

Ref.	IL_1, IL_2, dB	RL_1, RL_2, dB	FBW_1, FBW_2, %	f_1, f_2, GHz	Area (λ_g^2)
this work	0.12, 0.18	21, 17	16.4, 26	3.5, 5	0.0370
[1]	1.4, 2.3	15, 20	6.1, 4	1.05, 1.76	0.0890
[2]	1, 0.9	20, 20	6.1, 5.8	2.3, 2.72	0.1270
[3]	0.4, 0.42	20, 20	3.6, 3.4	1.8, 2.45	0.0957
[4]	—	29, 38	6.89, 6.56	2.35, 2.59	0.0820
[5]	1.2, 1.5	—	4.1, 3.74	1.95, 2.14	0.1360
[6]	0.6, 0.9	11.3, 12.4	—	2.6, 6	0.0820
[7]	2.2, 2.1	11.9, 12	2.8, 1.9	1.8, 2.4	0.0640
[8]	1.32, 0.95	32.8, 32.9	4.97, 8	1.81, 2.44	0.0960
[9]	2.1, 2.1	20, 20	4.2, 5.1	1.75, 1.85	0.0700
[10]	1.83, 1.52	—	8, 9.2	1.1, 1.3	0.7000
[11]	1.43, 1.59	22, 22	—	2.44, 2.53	0.2780
[12]	0.14, 0.16	18.5, 20	11, 7.1	1.8, 2.4	0.0220
[13]	0.36, 0.44	23.75, 23.74	—	2.88, 3.29	0.0280
[14]	0.28, 0.29	21.2, 24.3	3.2, 3.2	0.8, 0.9	0.0100
[16]	1.3, 1.45	20, 23	11, 13	8.3, 10	0.0710
[17]	0.7, 0.5	19.6, 22	—	0.9, 2.6	0.0170
[18]	1.45, 1.55	13, 30	5.96, 8.87	1.65, 1.75	0.0290
[19]	4.9, 3.9	16.8, 14	2.2, 3.2	8.75, 9.4	4.6900
[20]	0.25, 0.26	18.45, 17.47	—	2.12, 3.94	0.0380
[21]	0.17, 0.30	19, 21	12.5, 4.1	0.78, 1.85	0.0260
[22]	0.1, 0.16	35, 23	16.8, 11	1.6, 2.1	0.0540

Table 2 Harmonic attenuation of this work in comparison with the previous diplexers (*: approximated values)

Ref.	Last attenuated harmonics	*N*th suppressed harmonic	Maximum harmonic level
this work	44 GHz ($12f_1$)	12th	−17 dB
	20 GHz ($5.7f_1$)	5th	−20 dB
[1]	4 GHz ($2.8f_1$)	2nd	−20 dB
[2]	4 GHz ($1.73f_1$)	1st	−20 dB*
[3]	no	no	no
[4]	no	no	no
[5]	2.5 GHz ($2.08f_1$)	2nd	−30 dB
[6]	no	no	no
[7]	5 GHz ($2.77f_1$)	2nd	−35 dB*
[8]	no	no	No
[9]	2.4 GHz ($1.37f_1$)	1st	−10 dB
[10]	1.6 GHz ($1.5f_1$)	1st	−20 dB
[11]	5 GHz ($2f_1$)	2nd	−20 dB
[12]	6.48 GHz ($3.6f_1$)	3rd	−20 dB
[13]	no	no	no
[14]	2.2 GHz ($2.75f_1$)	2nd	−30 dB
[15]	9 GHz ($2.5f_1$*)	2nd	−20 dB
[21]	4 GHz ($5.1f_1$)	5th	−15 dB
[22]	4 GHz ($2.5f_1$)	2nd	−20 dB

a low group delay in a microstrip diplexer is harder than microstrip filters.

The proposed structure includes two stub-loaded hairpins and spiral cells. The patch structures have capacitance features while the spirals are compact inductors. The connected inductors and capacitors can create TZs at the special frequencies in the stopband, which are the TZ frequencies. At a TZ frequency, the values of inductors and capacitors are adjusted to create an open circuit between the input and output ports. From the *LC* model of the proposed resonator and at the special frequencies, the admittance from the input port to the output port should be zero to obtain TZs frequencies. Having an open circuit is possible for the high values of L_1 or L_4. As presented in Fig. 6, the coupling structures can create some capacitors. The equivalent capacitors of coupling structures are very small in fF. Therefore, these capacitors can create an open circuit between the input and output terminals which is another way to have TZs.

4 Conclusion

In this work, a novel high-performance microstrip diplexer is presented for IEEE 802.16 WiMAX and wireless applications. To design the proposed diplexer, first we proposed a novel resonator. Then, a BPF with a good performance in terms of low group delay and sharp frequency response was designed using the presented resonator. Finally, by integrating two similar BPFs with different dimensions, a microstrip diplexer was achieved. In comparison with the previous diplexers, the proposed diplexer has good

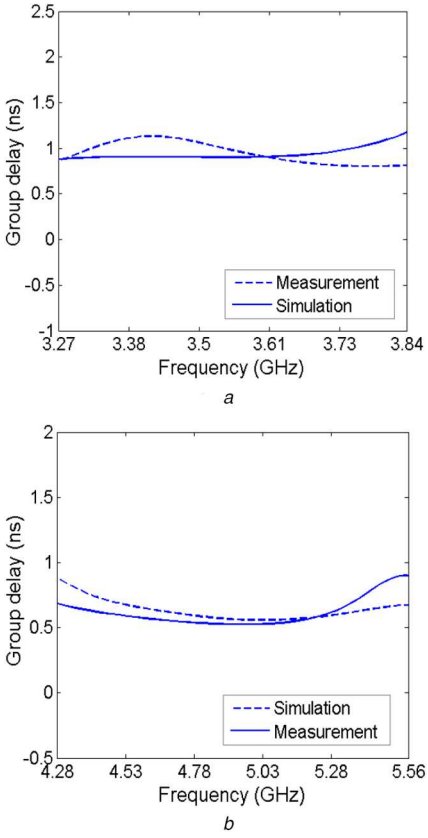

Fig. 10 *Group delay at the*
(a) Lower passband, ***(b)*** Upper passband

Table 3 Comparison between this work and the previous diplexers and filters in terms of group delay and flatness

Ref.	Number of channels	Type	Max. group delay of all channels, ns
this work	2	bandpass–bandpass diplexer	1.12
[6]	2	bandpass–bandpass diplexer	2.98
[12]	2	bandpass–bandpass diplexer	3.14
[15]	2	bandpass–bandpass diplexer	1.75
[23]	3	triple-band BPF	3.67
[24]	4	dual/quad-band filters	8
[25]	2	dual-band BPF	2.5
[26]	3	tri-band BPF	8
[20]	2	bandpass–bandpass diplexer	4
[21]	2	bandpass–bandpass diplexer	5.1
[22]	2	bandpass–bandpass diplexer	2.6

performance in terms of low insertion losses at all channels, good return losses, sharp frequency response, suppressed harmonics, the lowest group delay, wide and flat channels, the widest stopband rejection, and several TZs.

5 References

[1] Feng, W., Zhang, Y., Che, W.: 'Tunable dual-band filter and diplexer based on folded open loop ring resonators', *IEEE Trans. Circuit Syst.*, 2017, **64**, pp. 1047–1051, https://doi.org/10.1109/TCSII.2016.2634555

[2] Huang, F., Wang, J., Zhu, L.: 'Wu W. Compact microstrip balun diplexer using stub-loaded dual-mode resonators', *IET Electron. Lett.*, 2016, **52**, pp. 1994–1996, https://doi.org/10.1049/el.2016.3302

[3] Bui, D.H.N., Vuong, T.P., Allard, B., *et al.*: 'Compact low-loss microstrip diplexer for RF energy harvesting', *Electron. Lett.*, 2017, **53**, pp. 552–554, https://doi.org/10.1049/el.2017.0022

[4] Yang, F., Guan, X., Zhu, L., *et al.*: 'Compact microstrip diplexer for 4G wireless communication'. Progress in Electromagnetics Research Symp. Proc., Guangzhou, China, 2014, vol. 25, pp. 599–602, ISBN: 978-1-934142-28-8

[5] Guan, X., Yang, F., Liu, H., *et al.*: 'Compact and high-isolation diplexer using dual-mode stub-loaded resonators', *IEEE Microw. Wirel. Compon. Lett.*, 2014, **6**, pp. 385–387, https://doi.org/10.1109/LMWC.2014.2313591

[6] Noori, L., Rezaei, A.: 'Design of a microstrip diplexer with a novel structure for WiMAX and wireless applications', *AEU-Int. J. Electron. Commun.*, 2017, **77**, pp. 18–22, https://doi.org/10.1016/j.aeue.2017.04.019

[7] Yan, J.-M., Zhou, H.-Y., Cao, L.-Z.: 'Compact diplexer using microstrip half- and quarter wavelength resonators', *IET Electron. Lett*, 2016, **52**, (19), pp. 1613–5165, https://doi.org/10.1049/el.2016.2127

[8] Chinig, A., Zbitou, J., Errkik, A., *et al.*: 'Microstrip diplexer using stepped impedance resonators', *Wirel. Pers. Commun.*, 2015, **84**, pp. 2537–2548, https://doi.org/10.1007/s11277-015-2718-2

[9] Peng, H., Chiang, Y.: 'Microstrip diplexer constructed with new types of dual-mode ring filters', *IEEE Microw. Wirel. Compon. Lett.*, 2015, **25**, pp. 7–9, https://doi.org/10.1109/LMWC.2014.2365740

[10] Chen, D., Zhu, L., Bu, H., *et al.*: 'A novel planar diplexer using slot line-loaded microstrip ring resonator', *IEEE Microw. Wirel. Compon. Lett.*, 2015, **25**, pp. 706–708, https://doi.org/10.1109/LMWC.2015.2479836

[11] Xiao, J.K., Zhu, M., Li, Y., *et al.*: 'High selective microstrip bandpass filter and diplexer with mixed electromagnetic coupling', *IEEE Microw. Wirel. Compon. Lett.*, 2015, **25**, pp. 781–783, https://doi.org/10.1109/LMWC.2015.2495194

[12] Rezaei, A., Noori, L.: 'Compact low-loss microstrip diplexer using novel engraved semi-patch cells for GSM and WLAN applications', *AEU-Int. J. Electron. Commun.*, 2018, **87**, pp. 158–163, https://doi.org/10.1016/j.aeue.2018.02.022

[13] Rezaei, A., Noori, L., Mohammadi, H.: 'Design of a miniaturized microstrip diplexer using coupled lines and spiral structures for wireless and WiMAX applications', *Analog Integr. Circuits Signal Process.*, 2019, **98**, pp. 409–415, https://doi.org/10.1007/s10470-018-1365-4

[14] Rezaei, A., Noori, L.: 'Novel compact microstrip diplexer for GSM applications', *Int. J. Microw. Wirel. Technol.*, 2018, **10**, pp. 313–317, https://doi.org/10.1017/S1759078718000168

[15] Deng, H.W., Zhao, Y.J., Fu, Y., *et al.*: 'Compact and high isolation microstrip diplexer for broadband and WLAN applications', *Prog. Electromagn. Res.*, 2013, **133**, pp. 555–570, https://doi.org/10.2528/PIER12092303

[16] Dembele, S.N., Bao, J., Zhang, T., *et al.*: 'Compact microstrip diplexer based on dual closed loop stepped impedance resonator', *Progr. Electromagn. Res. C*, 2019, **89**, pp. 233–241

[17] Roshani, S., Roshani, S.: 'Design of a very compact and sharp bandpass diplexer with bended lines for GSM and LTE applications', *AEU – Int. J. Electron. Commun.*, 2019, **99**, pp. 354–360, https://doi.org/10.1016/j.aeue.2018.12.014

[18] Danaeian, M.: 'Miniaturized half-mode substrate integrated waveguide diplexer based on SIR–CSRR unit-cell', *Analog Integr. Circuits Signal Process.*, 2020, **102**, pp. 555–561, https://doi.org/10.1007/s10470-019-01528-5

[19] Chashmi, M.J., Rezaei, P., Kiani, N.: 'Y-shaped graphene-based antenna with switchable circular polarization', *Optik – Int. J. Light Electron. Opt.*, 2020, **200**, p. 1633213, https://doi.org/10.1016/j.ijleo.2019.163321

[20] Rezaei, A., Yahya, S.I., Noori, L., *et al.*: 'Design and fabrication of a novel compact low-loss microstrip diplexer for WCDMA and WiMAX applications', *J. Microw., Optoelectron. Electromagn. Appl.*, 2019, **18**, (4), pp. 482–491

[21] Rezaei, A., Yahya, S.I., Jamaluddin, M.H.: 'A novel microstrip diplexer with compact size and high isolation for GSM applications', *AEU-Int. J. Electron. Commun.*, 2020, **114**, p. 153018, https://doi.org/10.1016/j.aeue.2019.153018

[22] Rezaei, A., Yahya, S.I., Noori, L.: 'Design of a novel wideband microstrip diplexer using artificial neural network', *Analog Integr. Circuits Signal Process.*, 2019, **101**, pp. 1, pp. 57–66, https://doi.org/10.1007/s10470-019-01510-1

[23] Wibisono, G., Firmansyah, T., Syafraditya, T.: 'Design of triple-band bandpass filter using cascade tri-section stepped impedance resonators', *J. ICT Res. Appl.*, 2016, **10**, pp. 43–56, http://dx.doi.org/10.5614%2Fitbj.ict.res.appl.2016.10.1.4

[24] Lin, S.-C.: 'Microstrip dual/quad-band filters with coupled lines and quasi-lumped impedance inverters based on parallel-path transmission', *IEEE Trans. Microw. Theory. Tech.*, 2011, **59**, pp. 1937–1946, https://doi.org/10.1109/TMTT.2011.2142191

[25] Sarkar, P., Ghatak, R., Poddar, D.-R.: 'A dual-band bandpass filter using SIR suitable for WiMAX band'. Proceeding of the Int. Conf. on Information and Electronics Engineering IPCSIT, Singapore, 2011, vol. 6, pp. 70–74

[26] Liu, Y.: 'A tri-band bandpass filter realized using tri-mode T-shape branches', *Prog. Electromagn. Res.*, 2010, **105**, pp. 425–444, http://dx.doi.org/10.2528/PIER10010902